Chemical Physics 539 (2020) 110929

Contents lists available at ScienceDirect

Chemical Physics

journal homepage: www.elsevier.com/locate/chemphys

Size dependence in the electronic and optical properties of a BN analogue of two-dimensional graphdiyne: A theoretical study

İskender Muz[a], Fahrettin Göktaş[b], Mustafa Kurban[c,*]

[a] Department of Mathematics and Science Education, Nevşehir Hacı Bektaş Veli University, 50300 Nevşehir, Turkey
[b] Department of Energy System Engineering, Ankara Yıldırım Beyazıt University, 06170 Ankara, Turkey
[c] Department of Electrical and Electronics Engineering, Kırşehir Ahi Evran University, 40100 Kırşehir, Turkey

ARTICLE INFO

Keywords:
Graphdiyne
BNdiyne
2D sheets
DFTB

ABSTRACT

In this study, we propose a new type of a BN analogue of two-dimensional (2D) graphdiyne. By DFTB, we carried out the changes in the electronic and optical properties of BNdiyne based on size. Higher binding energies with increase size ensure an increase in the stability of BNdiyne. Considerable decrease in the energy gap from 1.09 eV to 0.02 eV suggests BNdiyne transforms from a semiconductor to metal, thus an increase in electrical conductivity. The HOMO energy of BNdiyne with size contributes the stability. The increase in the size induces a decrease in adiabatic electron affinity and chemical hardness, but an increase in the refractive index, adiabatic ionization potential, electrophilicity index and maximum amount electronic charge index which enhance the energy stability of the BNdiyne during charge transfer. These findings herein indicate that new 2D-BNdiyne can be used in promising applications from nanosensors to solar cell applications.

1. Introduction

Carbon-based materials (CBNs) have attracted intense scrutiny in diverse fields of applications due to their unique structure and electronic properties. Among them, graphdiyne (GDY), which has unique two-hybrid state ($sp - sp^2$), uniform pores, and highly π-conjugated structure [1,2], has induced much interest in many applications such as lithium-ion storage [3], nanocomposite photocatalyst [4], the anode of lithium and rechargeable batteries [5,6], clean energy [7], and spintronics [8,9].

GDY, a novel 2D non-natural carbon allotrope containing hexagonal carbon rings connected by diacetylene bonds [1], has been successfully synthesized in experiments [10]. GDY exhibits high electron mobility at room temperature owing to its bandgap of 0.46 eV [11,12], thus it has a high electrical conductivity [13]. With the properties mentioned above, an electrochemical actuator based on GDY has been fabricated with a high electromechanical transduction efficiency of up to 6.03% [14]. GDY as electrode has been performed for electrochemical supercapacitor [15]. Besides, the ultrathin GDY nanofilms considerably improve the coulombic efficiency and long-term cycling performance of Li metal battery [16]. Integrating ultrathin GDY sheets on silicon electrodes also exhibits high-performance silicon anode [17]. On the other hand, a novel GDY-ZnO nanohybrid was examined on the degradation of methylene blue and rhodamine B for photocatalytic applications [18].

Tunability in the electronic structure and optical properties of CBNs is possible with a dopant atom or molecule [19–21]. Among dopant atoms, in general, nitrogen (N)-and boron (B)-doped CBNs have been preferred, because the electrons can be injected into the materials by N atom [22] and thus tuning the properties. Herein, *N*-doped CBNs have been extensively studied both theoretically and experimentally [23–27] because *N*-doped GDY has more desirable properties than undoped GDY. The literature review shows that dopant N induces an increase in the performance of GDY electrochemical electrodes for new energy fields, such as fuel cells, batteries, solar cells, Li/Na-ion capacitors [28,29]. B/*N*-doped GDY can be used as superior supercapacitor electrode [30]. The *N*-doped GDY and porous GDY can be used as excellent metal-free catalysts for oxygen reduction [31,32]. The local structures of *N*-doped GDY are shown based on computational X-ray spectroscopy [33]. On the other hand, B-GDY based materials are suggested as promising candidates for Li, Na and K ion batteries [34]. In the literature, many studies have been performed to investigate the influence of size and doping of nanomaterials on their physical/chemical properties to design devices with improved performance [19,35–40]. The main conclusion from those studies is that at nanoscale the size plays a significant role. Herein, we systematically investigated the changes in the electronic and optical properties of BNdiyne based on the size for the first time. In this context, we explore the binding energy, adiabatic

* Corresponding author.
E-mail addresses: mkurbanphys@gmail.com, mkurban@ahievran.edu.tr (M. Kurban).

https://doi.org/10.1016/j.chemphys.2020.110929
Received 22 May 2020; Received in revised form 5 July 2020; Accepted 16 July 2020
Available online 20 July 2020

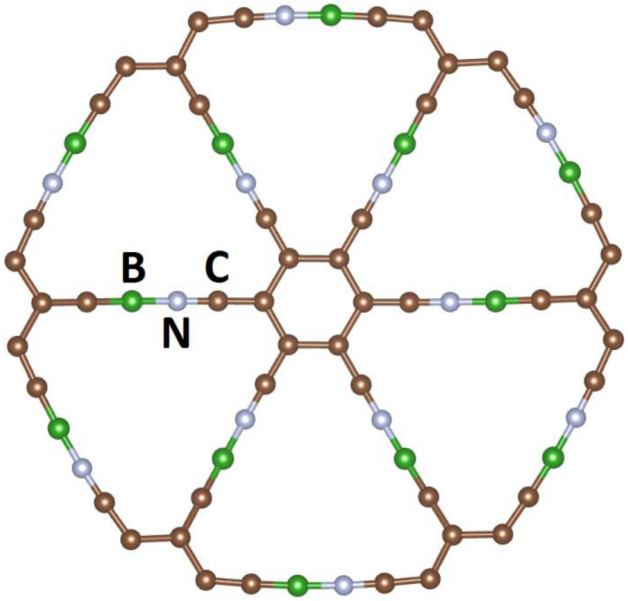

Fig. 1. (Colour online) The optimized geometry of 1-BNdiyne computed by DFTB method.

ionization potential, adiabatic electron affinity, HOMO, LUMO, HOMO-LUMO energy gap, the density of state, refractive index, electron localization function, Hirshfeld charge analyses, quantum chemical descriptors such as chemical hardness and potential, the maximum amount of electronic charge index, and electrophilicity index by density-functional tight-binding (DFTB) theory.

2. Computational details

The changes in the electronic and optical properties of BNdiyne based on size have been investigated using DFTB implemented in DFTB + code [41] with the matsci [42] set of Slater parameters. There has been previous works using full DFT and wavefunction-based methods on the base GDY structures [43,44] however, DFT limited to molecular systems made up of a small number of atoms when compared to DFTB which is also faster than DFT. Besides, our previous study and benchmarks showed that DFTB gives good match to DFT for GDY structures [45].

The optimized geometry of 1-BNdiyne which is the most stable structure is indicated in Fig. 1. The other structures are given in Fig. S2-S6 in Supporting information. The number of atoms changes from 72 (for $n = 1$, initial geometry with hexagonal structure) to 504 atoms (for $n = 7$). The binding energies E_b are calculated as follows:

$$E_b = (n_C \times E_C + n_B \times E_B + n_N \times E_N - E_{total})/(n_C + n_B + n_N) \quad (1)$$

where E_{total} is the total energy of n-BNdiyne ($n = 1$–7) models. E_C, E_B and E_N are the single particle energy of C, B and N atoms. n_C, n_N and n_H also are the numbers of C, N and H atoms. The adiabatic ionization potential (*AIP*) and adiabatic electron affinity (*AEA*) are calculated as follows: $[AIP = E^{cation} - E^{neutral}]$ and $[AEA = E^{neutral} - E^{anion}]$. Here, *AIP* is the difference in energy between cation (E^{cation}) and neutral ($E^{neutral}$) structures at their respective equilibrium geometries. *AEA* is the difference in energy between anion (E^{anion}) and neutral ($E^{neutral}$) structures at their respective equilibrium geometries. On the other hand, the HOMO/LUMO energies can be considered converged with respect to Pearson's theorem [46–48] by $I \approx -E_{HOMO}$ and $A \approx -E_{LUMO}$ and, consequently, properties such as chemical hardness (η), electrophilicity index (ω), maximum amount of electronic charge index (ΔN_{tot}) can be calculated as follows: $[\eta = (I - A)/2]$, $[\omega = (\frac{(I+A)}{2})^2/2\eta]$ and $[\Delta N_{tot} = -(I + A)/2\eta]$.

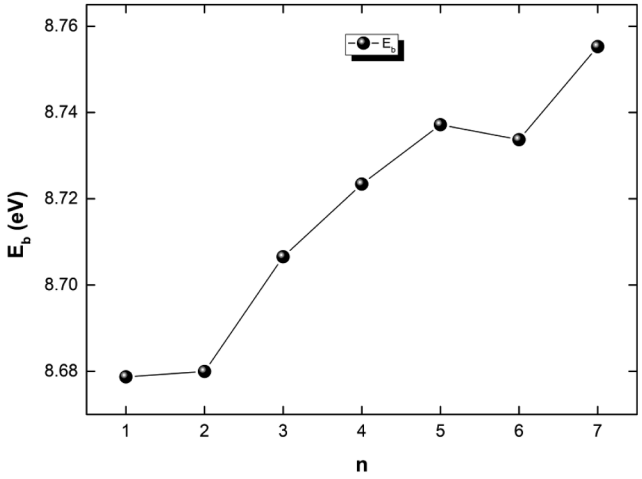

Fig. 2. (Colour online) Binding energy per atom (E_b) for n-BNdiyne ($n = 1$–7) models.

Table 1
The electronic and reactivity properties of n-BNdiyne ($n = 1$–7) periodic models. All values are eV.

	n						
	1	**2**	**3**	**4**	**5**	**6**	**7**
E_b	8.68	8.68	8.71	8.72	8.74	8.73	8.76
AIP	6.29	5.88	5.73	5.53	5.42	5.49	5.35
AEA	3.11	4.11	4.26	4.41	4.44	4.50	4.51
HOMO	−5.23	−5.16	−5.12	−4.99	−4.95	−5.04	−4.95
LUMO	−4.14	−4.90	−4.91	−4.95	−4.92	−4.97	−4.93
E_f	−4.69	−5.03	−5.01	−4.97	−4.93	−5.00	−4.94
E_g	1.09	0.25	0.21	0.04	0.02	0.07	0.02
η	1.59	0.88	0.73	0.56	0.49	0.49	0.42
ω	6.94	14.13	17.00	22.01	24.68	25.24	28.90
ΔN_{tot}	2.95	5.65	6.80	8.86	10.01	10.11	11.73

3. Results and discussions

3.1. Structure, energy and stability

The calculated binding energy per atom (E_b) for n-BNdiyne ($n = 1$–7) models is shown in Fig. 2 and listed in Table 1. The value of BNdiyne ($n = 1$) is calculated to be 8.68 eV. With an increase in the size, E_b increases slightly to 8.76 eV with the number of linking BNdiyne units, and thus 7-BNdiyne is a little more stable than the other models.

The HOMO/LUMO levels and HOMO-LUMO energy gap (E_g) for n-BNdiyne ($n = 1$–7) models are plotted in Fig. 3. The HOMO and LUMO energies of the BNdiyne ($n = 1$) are about −5.23 and −4.14 eV, and so E_g is found to be 1.10 eV for $n = 1$. However, LUMO level for $n = 2$ model shifts to lower energy level, and thus $E_g$decreases dramatically to 0.25 eV (see Table 1). Later, the energy level of HOMO increase generally in range of $n = 3$–7, while that of LUMO remains constant. Therefore, E_g is gradually decreased by increasing the number of BNdiyne units. Small values of E_g cause high electrical conductivity and, consequently, the electrical conductivity changes dramatically with the number of linking BNdiyne units. Therefore, n-BNdiyne models could be recommended as highly sensitive materials for the use of nanosensors. It is noteworthy to mention that the HOMO-LUMO energy gap in n-BNdiyne models can be tuned by changing the number of models. Fig. 4 shows the density of states (DOS) of n-BNdiyne ($n = 1$–7) models. The DOS provides information about the localization of charges in various energy ranges along with BNdiyne models. Moreover, for BNdiyne models, maximum peaks are seen in different energy ranges

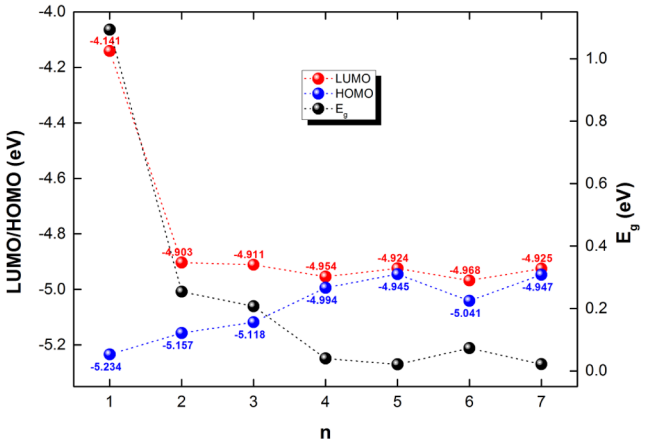

Fig. 3. (Colour online) HOMO, LUMO and HOMO-LUMO energy gap (E_g) for *n*-BNdiyne (*n* = *1–7*) models.

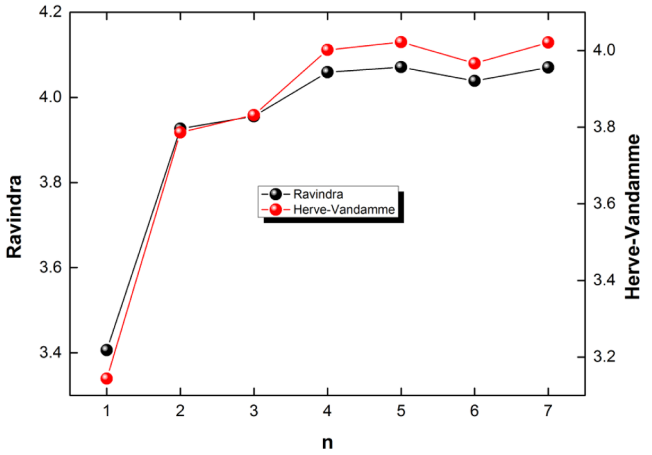

Fig. 5. (Colour online) Refractive indices based on Ravindra and Hervé-Vandamme relations of *n*-BNdiyne (*n* = *1–7*) models.

(-7.0/-6.0 eV, −2.5/-1.0 eV and 2.5/3.5 eV). This can be due to the overlapping of bands arising from C—C and B-N in the chains along with the BNdiyne models. Consequently, the DOS spectrum is significantly enhanced by increasing the number of BNdiyne units as it can be seen from the graphs of other models (*n* = *2–7*) compared to *n* = *1* (see Fig. 4). On the other hand, we find that the magnitude of DOS peaks of BNdiyne become higher with an increase in the size, which means stronger interaction of B/N dopants in BNdiyne, causing a metal–semiconductor transition. The similar behavior was observed in previous studies based on the CBNs [49,50], which arises from the spin-dependent splitting of carbon p-bands occurring in the gap.

3.2. Optical properties

We have examined the optical property of *n*-BNdiyne (*n* = *1–7*) models including refractive index (*n*). Ravindra [51] and Hervé and Vandamme [52] found relations between E_g and *n* in semiconductors $n = 4.084 - 0.62E_g$ and $n^2 - 1 = A^2/(E_g + B)^2$, respectively. *A* (13.6 eV) and *B* (3.4 eV) are a constant. The *n* of the *n*-BNdiyne (*n* = *1–7*) models is calculated from here and the results are plotted in Fig. 5. According to

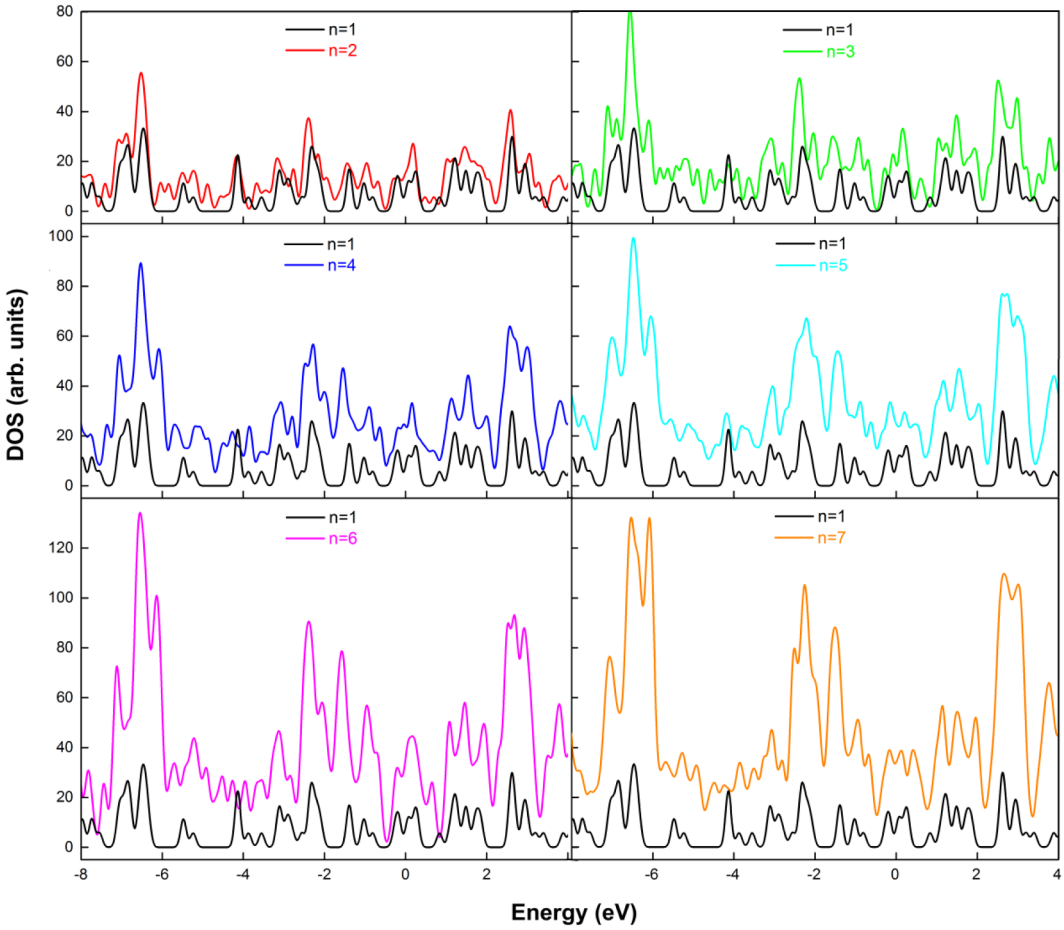

Fig. 4. (Colour online) Density of states (DOS) plots of *n*-BNdiyne (*n* = *1–7*) models.

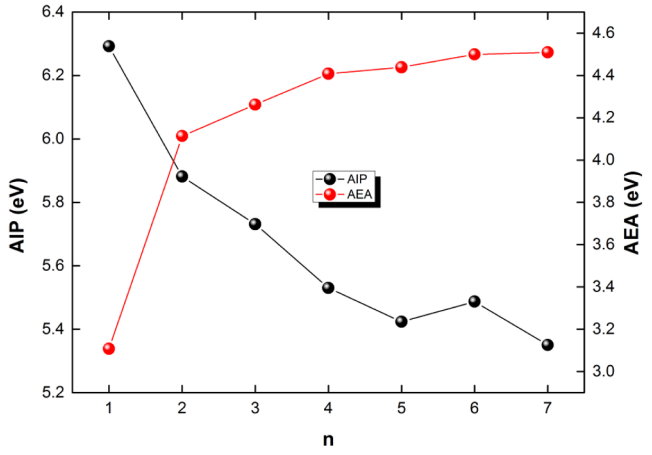

Fig. 6. (Colour online) Adiabatic ionization potential (AIP) and adiabatic electron affinity (AEA) of *n*-BNdiyne (*n* = *1–7*) models.

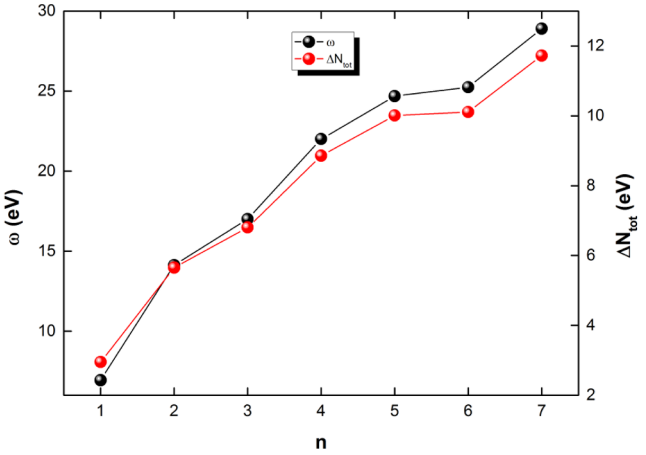

Fig. 8. (Colour online) Electrophilicity index (ω) and maximum amount electronic charge index (ΔN_{tot}) of *n*-BNdiyne (*n* = *1–7*) models.

Ravindra and Hervé and Vandamme relations, the *n* of the BNdiyne (*n* = *1*) is in the range of 3.2 to 3.4. Moreover, the *n* is increased up to *n* = *3* by increasing the number of BNdiyne unit but then remains constant in the range of *n* = *4–7*.

3.3. Electronic and reactivity properties

The AIP of the BNdiyne (*n* = *1*) is found to be 6.29 eV (see Table 1). AIP is generally decreased (see Fig. 6). This means that based on the number of BNdiyne units, the energy needed to remove an electron is decreased. On the other hand, the AEA of the BNdiyne (*n* = *1*) is calculated to be 3.11 eV (see Table 1). AEA shows a smooth upward trend with a sharp increase starting at *n* = *2* (see Fig. 6). We note that this rising in AEA can be a good option for optoelectronic applications due to the easier electron transfer. It is known that a hard structure corresponds to a large energy gap in the formalism of the maximum hardness principle [48]. In addition, a larger chemical hardness follows a larger ionization potential and a smaller electron affinity in the formalism of the Pearson principle [46,47]. Fig. 7 shows the chemical hardness (η) of *n*-BNdiyne (*n* = *1–7*) models. The η value of BNdiyne (*n* = *1*) is calculated to be 1.59 eV. Moreover, the η decreases significantly to 0.42 eV (see Table 1) with the number of linking BNdiyne units, thus indicating a lower impedance to charge flow and change in the energy gap. It also can be understood that the graph of η shows basically the same trend as that of AIP. Fig. 8 shows the electrophilicity index (ω)and maximum amount electronic charge index (ΔN_{tot})of *n*-BNdiyne (*n* = *1–7*) models.

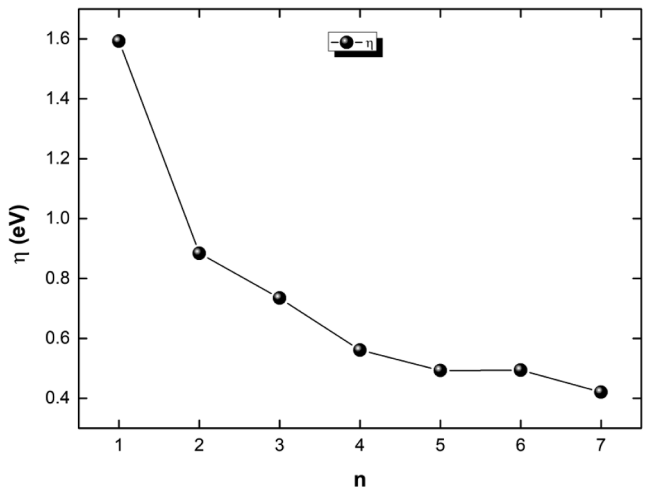

Fig. 7. (Colour online) Chemical hardness (η) of *n*-BNdiyne (*n* = *1–7*) models.

These indexes are used as a measure of the tendency of a given model to accept electron. The $\omega$and ΔN_{tot} values for BNdiyne (*n* = *1*) are calculated to be 6.94 eV and 2.95 eV (see Table 1), respectively. Moreover, ω and ΔN_{tot}show a smooth increasing trend as the number of BNdiyne units increase (see Fig. 8). Especially, ω is a term associated with the energy stability of the system during its charge transfer with the environment. We note that the increasing number of BNdiyne units could increase the structural strength of the system, and thus may cause a significant change in the structural properties.

We have examined the charge transfer of *n*-BNdiyne (*n* = *1–7*) models including Hirshfeld analysis. Fig. 9 shows the Hirshfeld charge analyses of *n*-BNdiyne (*n* = *1–7*) models. The majority of the charge of BNdiyne models is mainly on the B atoms. Despite the fact that the transfer of electrons goes from the more electropositive atoms to the more electronegative atoms, the charge is transferred from B to N and C. Note that the increasing number of BNdiyne units does not cause a significant change in the redistribution of charges.

4. Conclusions

In summary, we have carried out the effect of size on the electronic and optical properties of a new type of a BN analogue of 2D graphdiyne (BNdiyne) by DFT. Our calculated results show that the stability increases with increasing the size of BNdiyne due to changes in the binding energies. Increasing size effectively reduces the HOMO-LUMO

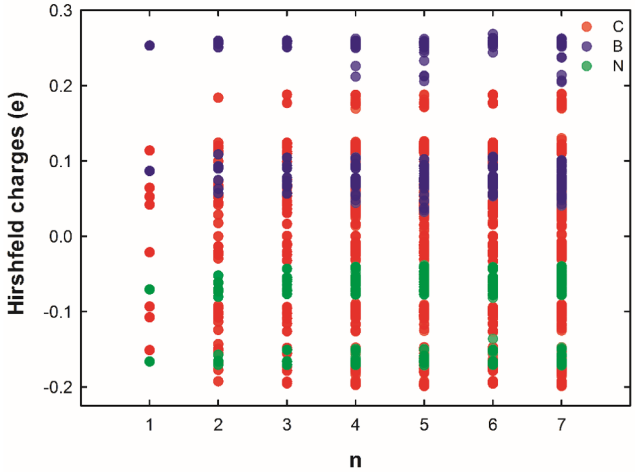

Fig. 9. (Colour online) Hirshfeld charge analyses of *n*-BNdiyne (*n* = *1–7*) models.

gaps in BNdiyne structures, so that BNdiyne transforms from a semiconductor to metal, thus an increase in electrical conductivity. The HOMO energy authenticates the stability of the BNdiyne with an increase in the size. The behavior of the size dependence of the adiabatic electron affinity and chemical hardness has been found to be a decreasing trend, however, an increase in the refractive index, adiabatic ionization potential, electrophilicity index and maximum amount electronic charge index, thus there is an enhancement in the energy stability of the BNdiyne during charge transfer. Overall, we hope that obtained results would provide an insight of experimental synthesis of this new material because many reported BN analogues of carbon-based materials have been synthesized successfully.

CRediT authorship contribution statement

İskender Muz: Investigation, Visualization, Writing - original draft, Writing - review & editing, Data curation. **Fahrettin Göktaş:** Investigation, Writing - review & editing. **Mustafa Kurban:** Supervision, Investigation, Methodology, Conceptualization, Writing - original draft, Writing - review & editing, Data curation, Validation, Software.

Declaration of Competing Interest

The authors declare that they have no known competing financial interests or personal relationships that could have appeared to influence the work reported in this paper.

Acknowledgment

The numerical calculations reported were partially performed at TUBITAK ULAKBIM, High Performance and Grid Computing Centre (TRUBA resources), Turkey.

Appendix A. Supplementary data

Supplementary data to this article can be found online at https://doi.org/10.1016/j.chemphys.2020.110929.

References

[1] M.M. Haley, S.C. Brand, J.J. Pak, Carbon networks based on dehydrobenzoannulenes: Synthesis of graphdiyne substructures, Angew. Chemie Int. Ed. 36 (1997) 836–838, https://doi.org/10.1002/anie.199708361.
[2] X. Gao, H. Liu, D. Wang, J. Zhang, Graphdiyne: synthesis, properties, and applications, Chem. Soc. Rev. 48 (2019) 908–936, https://doi.org/10.1039/c8cs00773j.
[3] S. Zhang, H. Du, J. He, C. Huang, H. Liu, G. Cui, Y. Li, Nitrogen-doped graphdiyne applied for lithium-ion storage, ACS Appl. Mater. Interfaces. 8 (2016) 8467–8473, https://doi.org/10.1021/acsami.6b00255.
[4] S. Wang, L. Yi, J.E. Halpert, X. Lai, Y. Liu, H. Cao, R. Yu, D. Wang, Y. Li, A novel and highly efficient photocatalyst based on P25-graphdiyne nanocomposite, Small. 8 (2012) 265–271, https://doi.org/10.1002/smll.201101686.
[5] C. Sun, D.J. Searles, Lithium storage on graphdiyne predicted by DFT calculations, J. Phys. Chem. C. 116 (2012) 26222–26226, https://doi.org/10.1021/jp309638z.
[6] A. Farokh Niaei, T. Hussain, M. Hankel, D. Searles, Sodium-intercalated bulk graphdiyne as an anode material for rechargeable batteries, J. Power Sources. 343 (2017) 354–363. Doi: 10.1016/jjpowsour.2017.01.027.
[7] Y. Jiao, A. Du, M. Hankel, Z. Zhu, V. Rudolph, S.C. Smith, Graphdiyne: a versatile nanomaterial for electronics and hydrogen purification, Chem. Commun. 47 (2011) 11843–11845, https://doi.org/10.1039/C1CC15129K.
[8] M. Zhang, X. Wang, H. Sun, N. Wang, Q. Lv, W. Cui, Y. Long, C. Huang, Enhanced paramagnetism of mesoscopic graphdiyne by doping with nitrogen, Sci. Rep. 7 (2017) 11535, https://doi.org/10.1038/s41598-017-11698-9.
[9] J. He, S.Y. Ma, P. Zhou, C.X. Zhang, C. He, L.Z. Sun, Magnetic properties of single transition-metal atom absorbed graphdiyne and graphyne sheet from DFT plus U calculations, J. Phys. Chem. C. 116 (2012) 26313–26321, https://doi.org/10.1021/jp307408u.
[10] G. Li, Y. Li, H. Liu, Y. Guo, Y. Li, D. Zhu, Architecture of graphdiyne nanoscale films, Chem. Commun. 46 (2010) 3256–3258, https://doi.org/10.1039/B922733D.
[11] M. Long, L. Tang, D. Wang, Y. Li, Z. Shuai, Electronic Structure and Carrier Mobility in Graphdiyne Sheet and Nanoribbons: Theoretical Predictions, ACS Nano. 5 (2011) 2593–2600, https://doi.org/10.1021/nn102472s.
[12] V. Nagarajan, R. Chandiramouli, Investigation of NH 3 adsorption behavior on graphdiyne nanosheet and nanotubes: A first-principles study, J. Mol. Liq. 249 (2018) 24–32, https://doi.org/10.1016/j.molliq.2017.11.007.
[13] L. Sun, P.H. Jiang, H.J. Liu, D.D. Fan, J.H. Liang, J. Wei, L. Cheng, J. Zhang, J. Shi, Graphdiyne: A two-dimensional thermoelectric material with high figure of merit, Carbon N. Y. 90 (2015) 255–259, https://doi.org/10.1016/j.carbon.2015.04.037.
[14] C. Lu, Y. Yang, J. Wang, R. Fu, X. Zhao, L. Zhao, Y. Ming, Y. Hu, H. Lin, X. Tao, Y. Li, W. Chen, High-performance graphdiyne-based electrochemical actuators, Nat. Commun. 9 (2018) 752, https://doi.org/10.1038/s41467-018-03095-1.
[15] K. Krishnamoorthy, S. Thangavel, J.C. Veetil, N. Raju, G. Venugopal, S.J. Kim, Graphdiyne nanostructures as a new electrode material for electrochemical supercapacitors, Int. J. Hydrogen Energy. 41 (2016) 1672–1678, https://doi.org/10.1016/j.ijhydene.2015.10.118.
[16] H. Shang, Z. Zuo, Y. Li, Highly Lithiophilic Graphdiyne Nanofilm on 3D Free-Standing Cu Nanowires for High-Energy-Density Electrodes, ACS Appl. Mater. Interfaces. 11 (2019) 17678–17685, https://doi.org/10.1021/acsami.9b03633.
[17] L. Li, Z. Zuo, H. Shang, F. Wang, Y. Li, In-situ constructing 3D graphdiyne as all-carbon binder for high-performance silicon anode, Nano Energy. 53 (2018) 135–143, https://doi.org/10.1016/j.nanoen.2018.08.039.
[18] S. Thangavel, K. Krishnamoorthy, V. Krishnaswamy, N. Raju, S.J. Kim, G. Venugopal, Graphdiyne-ZnO nanohybrids as an advanced photocatalytic material, J. Phys. Chem. C. 119 (2015) 22057–22065, https://doi.org/10.1021/acs.jpcc.5b06138.
[19] I. Muz, M. Kurban, A comprehensive study on electronic structure and optical properties of carbon nanotubes with doped B, Al, Ga, Si, Ge, N, P and As and different diameters, J. Alloys Compd. 802 (2019) 25–35, https://doi.org/10.1016/j.jallcom.2019.06.210.
[20] İ. Muz, F. Göktaş, M. Kurban, 3d-transition metals (Cu, Fe, Mn, Ni, V and Zn)-doped pentacene π-conjugated organic molecule for photovoltaic applications: DFT and TD-DFT calculations, Theor. Chem. Acc. 139 (2020) 23, https://doi.org/10.1007/s00214-020-2544-9.
[21] İ. Muz, M. Kurban, M. Dalkilic, DFT and TD-DFT studies of new pentacene-based organic molecules as a donor material for bulk-heterojunction solar cells, J. Comput. Electron. 19 (2020), https://doi.org/10.1007/s10825-020-01493-7.
[22] S.-S. Yu, W.-T. Zheng, Effect of N/B doping on the electronic and field emission properties for carbon nanotubes, carbon nanocones, and graphene nanoribbons, Nanoscale. 2 (2010) 1069–1082, https://doi.org/10.1039/c0nr00002g.
[23] B.K. Jiang, A.Y. Chen, J.F. Gu, J.T. Fan, Y. Liu, P. Wang, H.J. Li, H. Sun, J.H. Yang, X.Y. Wang, Corrosion resistance enhancement of magnesium alloy by N-doped graphene quantum dots and polymethyltrimethoxysilane composite coating, Carbon N. Y. 157 (2020) 537–548, https://doi.org/10.1016/j.carbon.2019.09.013.
[24] Y. Li, W. Ma, J. Sun, M. Lin, Y. Niu, X. Yang, Y. Xu, Electrochemical generation of Fe3C/N-doped graphitic carbon nanozyme for efficient wound healing in vivo, Carbon N. Y. 159 (2020) 149–160, https://doi.org/10.1016/j.carbon.2019.11.093.
[25] X. Qin, Y. Huang, K. Wang, T. Xu, S. Li, M. Zhao, Y. Wang, Q. Chen, Novel hexagonal Bi2O2CO3 porous nanoplate/nitrogen-doped graphene nanomaterials with enhanced electrochemical properties for oxygen reduction reaction in acidic media for fuel cells, Carbon N. Y. 152 (2019) 459–473, https://doi.org/10.1016/j.carbon.2019.06.028.
[26] N. Wanninayake, Q. Ai, R. Zhou, M.A. Hoque, S. Herrell, M. Guzman I, C. Risko, D. Y. Kim, Understanding the effect of host structure of nitrogen doped ultra-nanocrystalline diamond electrode on electrochemical carbon dioxide reduction, Carbon N. Y. 157 (2020) 408–419. https://doi.org/10.1016/j.carbon.2019.10.022.
[27] M. Kurban, Electronic structure, optical and structural properties of Si, Ni, B and N-doped a carbon nanotube: DFT study, Optik (Stuttg). 172 (2018) 295–301, https://doi.org/10.1016/j.ijleo.2018.07.028.
[28] H. Shang, Z. Zuo, H. Zheng, K. Li, Z. Tu, Y. Yi, H. Liu, Y. Li, Y. Li, N-doped graphdiyne for high-performance electrochemical electrodes, Nano Energy. 44 (2018) 144–154, https://doi.org/10.1016/j.nanoen.2017.11.072.
[29] X. Shen, Z. Yang, K. Wang, N. Wang, J. He, H. Du, C. Huang, Nitrogen-Doped Graphdiyne as High-capacity Electrode Materials for Both Lithium-ion and Sodium-ion Capacitors, ChemElectroChem. 5 (2018) 1435–1443, https://doi.org/10.1002/celc.201800300.
[30] W. Zeng, Y. Zhang, X. Liu, L. Qi, W. Kang, L. Fang, M. Zhou, B/N-doped graphdiyne as superior supercapacitor electrode with record high quantum capacitance, Appl. Surf. Sci. 523 (2020) 146468, , https://doi.org/10.1016/j.apsusc.2020.146468.
[31] Q. Lv, W. Si, J. He, L. Sun, C. Zhang, N. Wang, Z. Yang, X. Li, X. Wang, W. Deng, Y. Long, C. Huang, Y. Li, Selectively nitrogen-doped carbon materials as superior metal-free catalysts for oxygen reduction, Nat. Commun. 9 (2018) 3376, https://doi.org/10.1038/s41467-018-05878-y.
[32] Q. Lv, W. Si, Z. Yang, N. Wang, Z. Tu, Y. Yi, C. Huang, L. Jiang, M. Zhang, J. He, Y. Long, Nitrogen-Doped Porous Graphdiyne: A Highly Efficient Metal-Free Electrocatalyst for Oxygen Reduction Reaction, ACS Appl. Mater. Interfaces. 9 (2017) 29744–29752, https://doi.org/10.1021/acsami.7b08115.
[33] Y. Ma, J. Lin, X.-N. Song, C.-K. Wang, W. Hua, Y. Luo, Local structures of nitrogen-doped graphdiynes determined by computational X-ray spectroscopy, Carbon N. Y. 149 (2019) 672–678, https://doi.org/10.1016/j.carbon.2019.04.045.
[34] I. Muhammad, S. Wang, J. Liu, H. Xie, Q. Sun, Boron-graphdiyne as an anode material for Li, Na, and K ion batteries with high capacities and low diffusion barriers, J. Renew. Sustain. Energy. 11 (2019) 14106, https://doi.org/10.1063/1.5079928.
[35] M.J. Pitkethly, Nanometerials - The driving force, Mater. Today. 7 (2004) 20–29, https://doi.org/10.1016/S1369-7021(04)00627-3.
[36] H. Kurban, M. Kurban, M. Dalkılıç, Density-functional tight-binding approach for the structural analysis and electronic structure of copper hydride metallic nanoparticles, Mater. Today Commun. 21 (2019) 100648, , https://doi.org/10.1016/j.mtcomm.2019.100648.

[37] H. Gleiter, Nanostructured materials: basic concepts and microstructure, Acta Mater. 48 (2000) 1–29, https://doi.org/10.1016/S1359-6454(99)00285-2.
[38] C.M. Lieber, Z.L. Wang, Functional nanowires, MRS Bull. 32 (2007) 99–108, https://doi.org/10.1557/mrs2007.41.
[39] E. Sutter, P. Sutter, Phase diagram of nanoscale alloy particles used for vapor-liquid-solid growth of semiconductor nanowires, Nano Lett. 8 (2008) 411–414, https://doi.org/10.1021/nl0719630.
[40] İ. Muz, M. Kurban, Electronic structures and bonding of graphdiyne and its BN analogs: Transition from quasi-planar to planar sheets, J. Alloys Compd. 155987 (2020).
[41] B. Aradi, B. Hourahine, T. Frauenheim, DFTB+, a Sparse Matrix-Based Implementation of the DFTB Method, J. Phys. Chem. A. 111 (2007) 5678–5684, https://doi.org/10.1021/jp070186p.
[42] B. Lukose, A. Kuc, J. Frenzel, T. Heine, On the reticular construction concept of covalent organic frameworks, Beilstein J. Nanotechnol. 1 (2010) 60–70, https://doi.org/10.3762/bjnano.1.8.
[43] G. Luo, X. Qian, H. Liu, R. Qin, J. Zhou, L. Li, Z. Gao, E. Wang, W.-N. Mei, J. Lu, Y. Li, S. Nagase, Quasiparticle energies and excitonic effects of the two-dimensional carbon allotrope graphdiyne: Theory and experiment, Phys. Rev. B. 84 (2011) 075439, , https://doi.org/10.1103/PhysRevB.84.075439.
[44] S. Pari, A. Cuéllar, B.M. Wong, Structural and Electronic Properties of Graphdiyne Carbon Nanotubes from Large-Scale DFT Calculations, J. Phys. Chem. C. 120 (2016) 18871–18877, https://doi.org/10.1021/acs.jpcc.6b05265.
[45] İ. Muz, M. Kurban, The electronic structure, transport and structural properties of nitrogen-decorated graphdiyne nanomaterials, J. Alloys Compd. 842 (2020) 155983. Doi: 10.1016/j.jallcom.2020.155983.
[46] R.G. Pearson, Chemical hardness and density functional theory, J. Chem. Sci. 117 (2005) 369–377, https://doi.org/10.1007/BF02708340.
[47] R.G. Pearson, The electronic chemical potential and chemical hardness, J. Mol. Struct. Theochem. 255 (1992) 261–270, https://doi.org/10.1016/0166-1280(92)85014-C.
[48] R.G. Pearson, The principle of maximum hardness, Acc. Chem. Res. 26 (1993) 250–255, https://doi.org/10.1021/ar00029a004.
[49] L.N. Chen, F.P. Ouyang, S.S. Ma, X.Z. Wu, J. Xiao, H. Xu, First-principles investigation on B/N co-doping of metallic carbon nanotubes, Phys. Lett. Sect. A Gen. At. Solid State Phys. 374 (2010) 4343–4348, https://doi.org/10.1016/j.physleta.2010.08.015.
[50] M.U. Kahaly, U.V. Waghmare, Contrast in the electronic and magnetic properties of doped carbon and boron nitride nanotubes: A first-principles study, J. Phys. Chem. C. 112 (2008) 3464–3472, https://doi.org/10.1021/jp072340d.
[51] N.M. Ravindra, S. Auluck, V.K. Srivastava, On the penn gap in semiconductors, Phys. Status Solidi B. 93 (1979) K155–K160, https://doi.org/10.1002/pssb.2220930257.
[52] P.J.L. Herve, L.K.J. Vandamme, Empirical temperature-dependence of the refractive-index of semiconductors, J. Appl. Phys. 77 (1995) 5476–5477, https://doi.org/10.1063/1.359248.